Understanding Charge Transfer Mechanism on Effective Truxene-Based Porous Polymers-TiO_2 Hybrid Photocatalysts for Hydrogen Evolution

Antonio Valverde-González,[†] *Carmen G. López Calixto,*[$] *Mariam Barawi,*[$] *Miguel Gomez-Mendoza,*[b] *Víctor A. de la Peña O´Shea,*[$] *Marta Liras,*[*,$] *Berta Gómez-Lor,*[*,†] *Marta Iglesias*[*,†]

[†]Instituto de Ciencia de Materiales de Madrid. CSIC. C/ Sor Juana Inés de la cruz, 3. Madrid, Spain.

[$]Photoactivated Processes Unit, IMDEA Energy, Avda. Ramón de la Sagra 3, 28935, Móstoles, Madrid, Spain.

E mail: marta.liras@imdea.org, bgl@icmm.csic.es and marta.iglesias@icmm.csic.es

Keywords: porous polymers, solvent knitting, Truxene, hybrid materials, photocatalytic H_2 production, solar fuels

ABSTRACT: Truxene-based porous polymers synthesized through the simple "solvent knitting" strategy from hexamethyl or tribenzyl truxene-based monomers (TxPP1 and TxPP2), and their corresponding TxPP@TiO_2 hybrids are used as photocatalysts for H_2 production from water using methanol as sacrificial agent, under UV-Vis light. These polymers present higher hydrogen evolution rate (*HER*) than TiO_2, and remarkable thermo- and photo-stabilities. Hybrids TxPP-TiO_2 exhibited intensely enhanced photocatalytic activity compared to TiO_2 or TxPPs alone. In the presence of platinum (1%) as cocatalyst, *HER* from TxPP1@T-10 significantly boosted reaching values above 21000 $\mu mol.g^{-1}.h^{-1}$ which to the best of our knowledge, represents the highest *HER* reported for hybrids based on TiO_2 and conjugated porous polymers. Interestingly, small structural differences of the corresponding truxene monomers result in different photocatalytic behavior. We focused here on gaining insight on the charge transfer mechanism and rationalizing the different photocatalytic performances in order to establish clear structure-activity relationships. In fact, photoluminescence and transient absorption spectroscopy demonstrated that the remarkably enhanced photocatalytic activity of the most active hybrids (TxPP1@TiO_2) can be attributed to the efficiently photogenerated electron-hole separation by a direct Z-scheme mechanism, while lower

performance of TxPP2@TiO_2, is probably due to a less efficient heterojunction type II charge transfer mechanism.

INTRODUCTION

Photocatalytic hydrogen (H_2) production from the water splitting represents one of the most promising and challenging strategies for resolving the global energy and environmental problems associated to the use of fossil fuels.[1–3] Alternatively, titanium dioxide (TiO_2) has been widely used as photocatalyst for water splitting due its environmental friendliness, low cost, long-term stability against photo and chemical corrosion, and favorable energy levels to promote the water-splitting reaction.[4,5] Unfortunately, despite the advantages above mentioned, photocatalytic water-splitting efficiency of TiO_2 under solar energy is still quite low due to the inability of this material to absorb visible energy and to its high electron-hole recombination rate.[6] Coupling TiO_2 with other light-responsive semiconductors (such as graphitic carbon nitride, g-C_3N_4)[7] has demonstrated to be an effective way to improve its photocatalytic activity by enabling the charge carrier separation and extending its light absorption spectrum.[8,9] Recently conductive polymers[10,11] and their composites with inorganic semiconductors have emerged as promising alternatives.[12] Conjugated porous polymeric networks are particularly interesting because of their insoluble character and permanent porosity which render them very attractive for catalytic heterogeneous processes, while their π-delocalized systems provide the necessary photoactivity.[13–16] On the other hand, their optoelectronic properties can be readily tailored by the convenient choice of the monomers or by their rational post-functionalization in order to optimize their performance.[17,18] Although several hybrid materials based on porous polymers and inorganic semiconductors have been reported in the last few years,[4, 12] the fundamentals of the synergy observed in this kind of photocatalytic systems have been scarcely explored beyond those based on g-C_3N_4.

Until now, a great variety of π-conjugated molecules have been used as monomers in the construction of photoactive porous polymers.[17,19] Among them, we are interested in the truxene moiety. This highly stable trigonal molecule owns attractive photophysical and semiconducting properties, which are being extensively exploited by its incorporation in different light emitting and photovoltaic devices.[20] Interestingly conductive porous polymers (CPPs) obtained by covalently linking of truxene-building units have been found to show high specific surface area, thermal and chemical stability and excellent heterogeneous photocatalytic activity in the aerobic oxidative self-coupling of benzylamine even under natural sunlight illumination.[21,22] Inspired by these positive results, herein we investigate two covalently linked truxene-based porous polymers (starting from differently substituted truxene monomers, Scheme 1) and their corresponding hybrids with TiO_2 to be used as photocatalysts for light-driven hydrogen production from water. To unravel the differences in the HER from both hybrid system we have focused our investigation in the establishment of structure–activity relationships by means of photoluminescence experiments, TEM images and time resolve transient absorption spectroscopy (TAS).

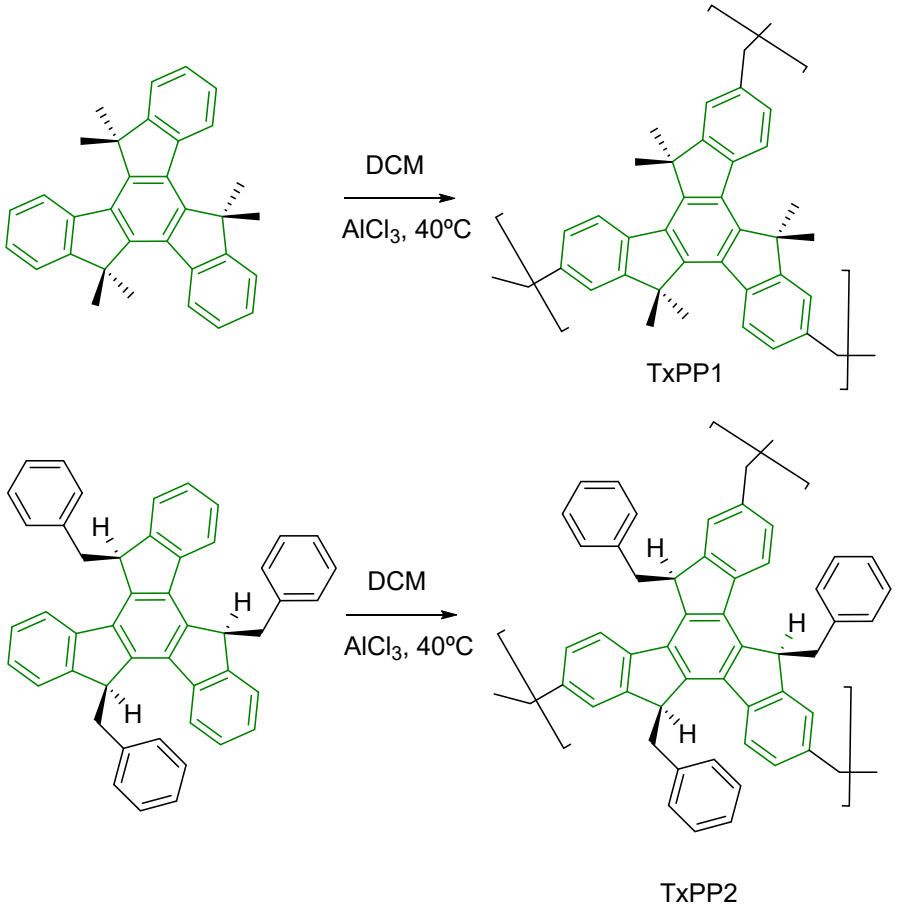

Scheme 1. Synthesis of truxene-based polymers.

RESULTS AND DISCUSSION

Synthesis of truxene-based polymers.

We have recently reported the simple multi-gram synthesis of porous truxene-based organic polymer TxPP1 (see Scheme 1), by $AlCl_3$ mediated coupling of hexamethyltruxene (TxMe) following what is known as a "knitting" protocol.[21] By using the same synthetic approach we have now synthesized a new polymer TxPP2, starting from a truxene functionalized in the 5,10,15 positions with three bulky benzyl groups in an all *syn* configuration (TxBn). The polymerization presumably occurs by Friedel-Crafts alkylation with the participation of CH_2Cl_2 molecules as electrophile providing methylene linkers. The tribenzyltruxene can be easily obtained by

alkylation of truxene in basic medium followed by isomerization of the *syn- anti* mixture to the most stable *syn*-isomer as previously reported.[23,24]

After purification, the polymer was obtained as an orange powder in 90% yield. Elemental analysis, ICP, EDX, and TGA confirm both the yield and that no residual elements from the coupling reaction are left (Table S1, Supporting Information). Please, note that polymers obtained through Suzuki or Sonogashira C-C-couplings often contain different quantities of residual Pd catalyst, which can alter their photocatalytic behavior.[25–27] In this case, the only possible metal impurity is aluminum, and its presence was discarded by EDX and ICP analysis.

Figure 1 shows the ^{13}C cross-polarization magnetic-angle spinning (CP/MAS) NMR, Fourier transform infrared (FT-IR) spectra, thermogravimetric analysis (TGA) and N_2 adsorption isotherms at 77K of both TxPP2 and TxPP1polymers (red and blue, respectively).

In the ^{13}C CP/MAS NMR spectrum the new polymers exhibit signals in the range of 120-140 ppm attributed to the aromatic carbons and in the range of 20-60 ppm corresponding to methylene carbons (benzylic and linker). FT-IR spectrum shows peaks at ~3020-2920 cm^{-1} corresponding to $\nu(C\text{-}H)$ vibrations, a peak at 1610-1600 cm^{-1} corresponding to $\nu(C=C)$ and peaks at 1445, 1395 and 849 cm^{-1} which are attributed to the vibrations of the truxene skeleton. TxPP2 shows the same high thermal stability under air atmosphere as TxPP1. As can be seen, decomposition starts around 350 ºC and at 500 ºC, the polymers were totally degraded, the gain (5%) of weight about 300 ºC is in agreement with the easy oxidation of the methylene linkers.[21]

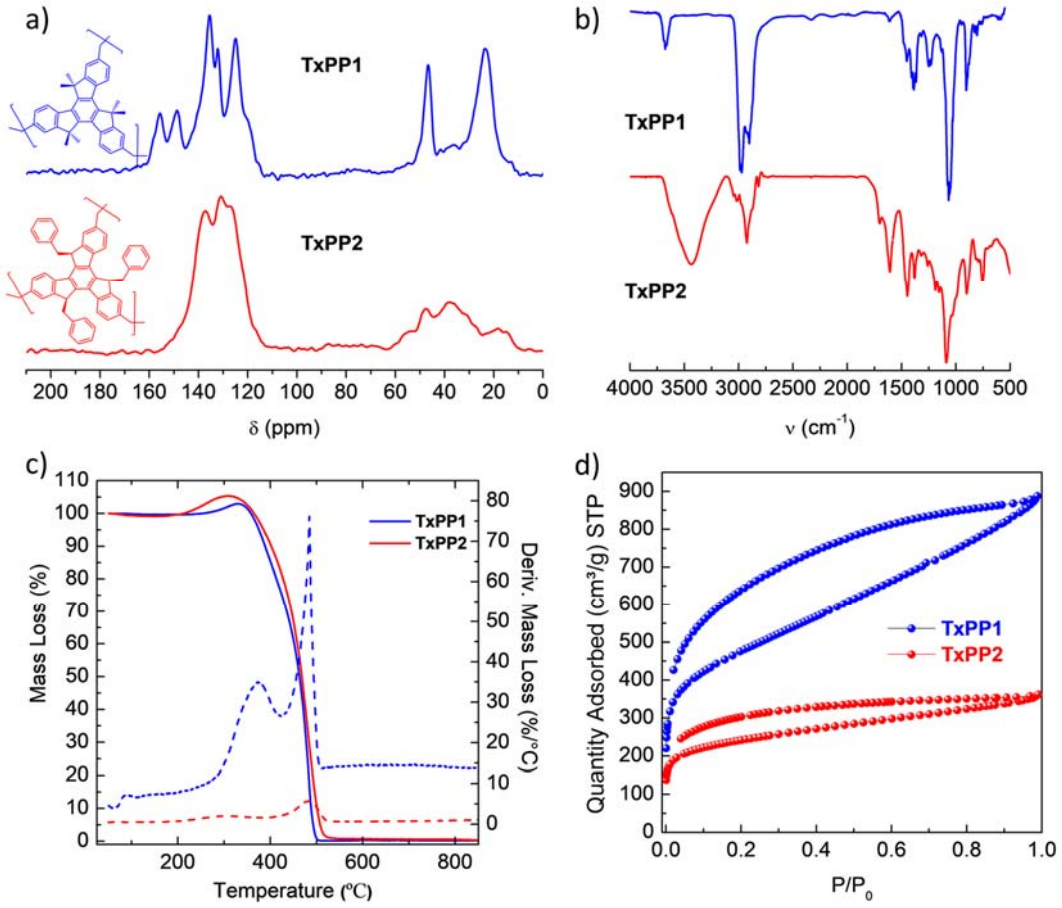

Figure 1. a) ^{13}C-NMR, b) FT-IR, c) TGA and d) N_2 isotherm adsorption for TxPP2 polymer compared with TxPP1.[15]

The surface area of TxPP2 obtained by Brunauer–Emmett–Teller (BET) equation is *ca.* 876 $m^2.g^{-1}$, significantly lower than that previously obtained for TxPP1 (*ca.* 1688 $m^2.g^{-1}$) (Table 1). This is probably due to higher steric hindrance introduced by the bulky benzyl substituent. Scanning electron microscopy (SEM) of TxPP2 shows a spherical morphology, as frequently observed in porous polymers (Figure S2, Supporting Information).

Table 1. Porous properties of truxene-PPs, bare TiO_2 and hybrid materials.

Polymer	SA_{BET} ($m^2.g^{-1}$)[a]	Pore volume ($cm^3.g^{-1}$)[b]	Pore size (nm)[c]
TxPP1	1688	1.37[c]	3.25[c]
TxPP2	876	0.55[c]	2.50[c]
TiO2[d]	117	0.45	11.5
TxPP1@T-10	92	0.45[e]	17.9[e]
TxPP2@T-10	96	0.36[e]	13.1[e]

[a]BET surface area calculated from the nitrogen adsorption isotherm. [b]At P/P_0: 0.99. [c]by DFT methods. [d]Bare TiO_2 BET surface area is included for comparative proposes. [e] by BJH method.

Photocatalytic activity

The photocatalytic activity of truxene polymers was evaluated in the hydrogen evolution reaction from water under UV-Vis irradiation (see spectrum of the irradiation source at Figure S3, Supporting Information) using 10 % methanol as sacrificial agent. Under these conditions, TxPP1 and TxPP2 show hydrogen evolution rates of 285 μmol.h^{-1}.g^{-1} and 116 μmol.h-1.g^{-1} respectively (entries 3 and 5, table 2) representing hydrogen production values 4.7 and 1.9-fold respectively higher than that obtained with TiO_2.

Since, it is very well known that noble metal co-catalysts, such as platinum, act as electron traps hindering the electron–hole recombination in artificial photosynthesis processes[28–30] we opted to add platinum to our materials. Thus, both polymers loaded with platinum nanoparticles, photodeposited from H_2PtCl_6 (1 wt. %), show a slight increase in the hydrogen evolution rate (*HER*) (*ca*. 320 μmol g^{-1}.h^{-1} and 134 μmol g^{-1}.h^{-1}, entries 4 and 6, table 2). Results, with and without loading of Pt, seem to be in the same order of other porous polymers described in the literature.[15,30–32] The increase of hydrogen production by Pt loading is usually more remarkable in TiO_2 and other inorganic semiconductors than in the organic counterparts.[33] In our hands, the *HER*

by TiO_2 loaded with the same amount of Pt increased up to 7620 μmol $g^{-1}.h^{-1}$, (entries 1-2, table 2). In order to analyze possible synergies between TiO_2 and polymers based on truxene, we prepared hybrid organic-inorganic materials. Bare TiO_2 was loaded with 5, 10 and 15 wt. % of TxPP1 (TxPP1@T-5, TxPP1@T-10 and TxPP1@T-15, respectively). In all cases the morphology of the hybrid is the same, showing tiny nanocrystals of TiO_2 decorating the surface of the polymers (Figure 2). The hybrid textural properties such as crystallinity and porosity were evaluated by means of powder x-ray diffraction (XRD) and N_2 adsorption measurements, respectively. As expected, TxPPs are amorphous and hybrid materials show the diffraction pattern of anatase (Figure S4). On the other hand, the adsorption properties of both hybrids are dominated by the titania (see Table 1), showing N_2 adsorption isotherms similar to bare TiO_2 (see Figure S5 at Supporting Information). This is indicative of the core shell structure of the hybrid materials, being the TiO_2 nanoparticles blocking the surface of both polymers.

TxPP1@T-10 shows the highest hydrogen production rate (*ca.* 388 μmol $g^{-1}.h^{-1}$), 4.7-fold higher than the sum of the photocatalytic activities of the bare materials. Meanwhile, the same proportion of polymer loading with TxPP2 shows also a synergy effect (*ca.* 100 μmol $g^{-1}.h^{-1}$) but lower than in the case of TxPP1 (see theoretical *HER* values without synergy in Table S2). Figure 3 depicts the kinetic profile of the reaction catalyzed by both hybrids at 10 wt.% of polymer loading and bare titania.

Table 2. Photocatalytic H_2 evolution rate (HER).

entry	Catalyst	Co-catalyst added	Sacrificial agent	Light source	HER ($\mu mol\ .g^{-1}.h^{-1}$)	Ref(year)
1	TiO_2	--			60	
2	TiO_2	1% Pt			7620	
3	TxPP1	--			285	
4	TxPP1	1% Pt			320	
5	TxPP2	--			116	
6	TxPP2	1% Pt			134	
7	TxPP1@T-5	--	10 vol.% MeOH	Hg Lamp	86	This work
8	TxPP1@T-10	--			388	
9	TxPP1@T-15	--			232	
10	TxPP2@T-10	--			100	
11	Pt/TxPP1@T-5	1% Pt			11460	
12	**Pt/TxPP1@T-10**	**1% Pt**			**21945**	
13	Pt/TxPP1@T-15	1% Pt			9600	
14	Pt/TxPP2@T-10	1% Pt			17980	
15	TiO_2@CMPBBT (6.7%)	0.5 Pt	TEOA solution	Xe-lamp (λ≥420 nm)	5933	35(2017)
	TiO_2				--	
	CMPBBT				333	
16	TiO_2@COP64 (10%)	3 wt. % Pt	20 vol.% MeOH	Xe-lamp	15020	36(2017)
	TiO_2				9200	
	COP64				0	
17	TiO_2@g-C_3N_4	Pt (amount no provided)	20 vol.% MeOH	Solar simulator	8931	37(2015)
	TiO_2				7557	
	g-C_3N_4				926.8	
18	polycathecol@TiO_2[a)]	--	5 vol% TEOA	Solar light	10925	38(2017)
19	B-BT-1,4-E@TiO_2[a)]	0.03% residual Pd	TEOA aq	Xe lamp (λ≥420 nm)	7333	39(2018)
20	TiO_2@B-BT-1,4-E	1wt%Au	10 vol% TEOA	Xe lamp (λ≥420 nm)	26640	40(2018)
21	BFA@TiO_2[a)]	residual Pd	TEOA aq	Xe lamp (λ≥420 nm)	3670	41(2019)

a) Note that in these cases the polymers are coating the TiO_2 nanocrystals

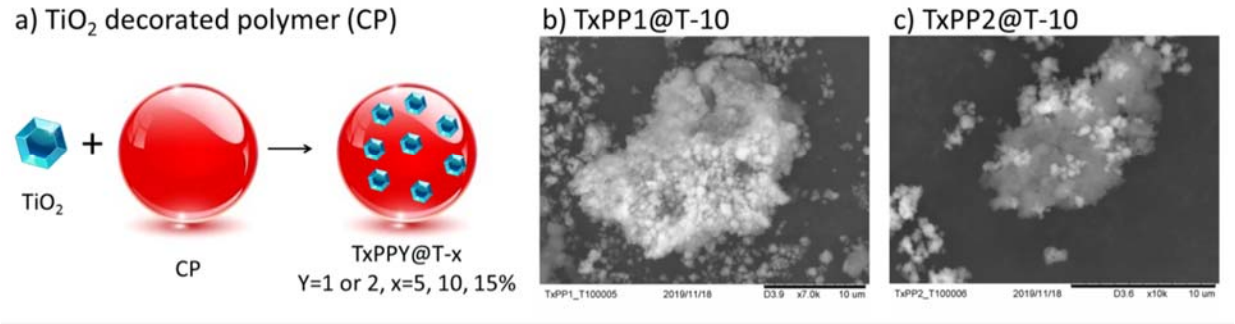

Figure 2. a) Cartoon describing the morphology of both hybrids; b) SEM image of TxPP1@T-10 hybrid material; c) SEM image of TxPP2@T-10 hybrid material.

With these results in hand, we decided to combine both approaches: the mixture of truxene polymers with TiO_2 and the loading effect of Pt. Interestingly, Pt-loaded hybrid catalysts showed a significant synergy effect in all different composites (Pt/TxPP1@T-5, Pt/TxPP1@T-10, Pt/TxPP1@T-15) being the hybrid material with 10% loading, the one that showed the highest H_2 production. Pt/TxPP1@T-10 and Pt/TxPP2@T-10 samples showed an impressive increased *HER* (*ca.* 21945 μmol g^{-1} h^{-1} and 17980 μmol g^{-1} h^{-1}) 2.9 and 2.4-fold respectively higher than Pt/TiO_2. Figure 4 depicts the kinetic profiles of these reactions. For comparative purposes, entries 15-21 at table 2 depict results from literature about hybrid materials based on conjugated polymers and titania. Note that this topic has been reviewed recently by Liras *et al.*[12] As far as we know, the hybrid material Pt/TxPP1@T-10 shows the highest *HER* reported up to now for hybrid materials based on TiO_2 and conjugated porous polymers. A higher *HER* in related systems have been only found in an hybrid material composed of a linear conjugated benzothiadiazole-based polymer (B-BT-1,4-E, entry 20) and TiO_2.[40] However, note that in this case, Au NPs are employed as cocatalyst taking advantage of the gold surface plasmon resonance (SPR), making the comparison not straightforward.

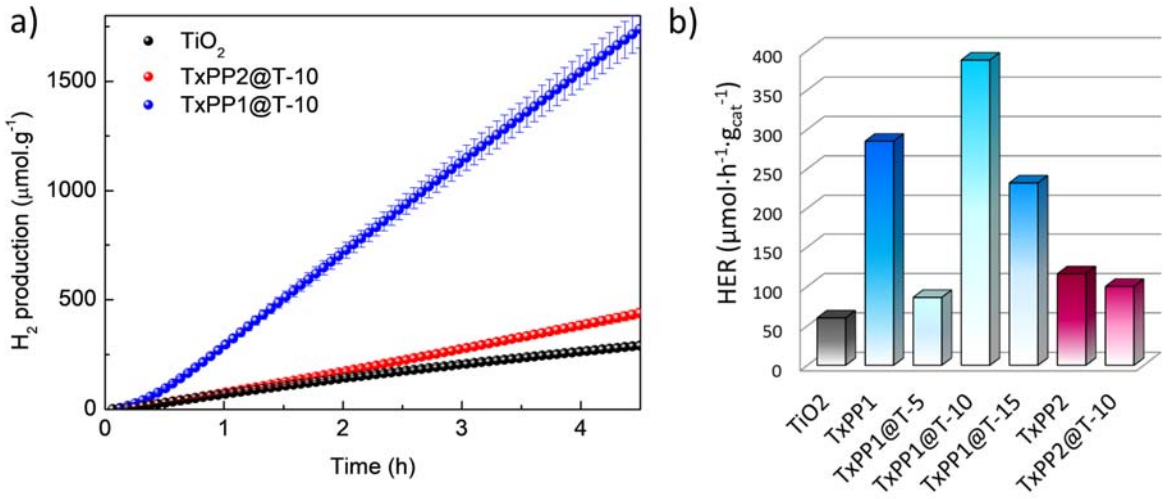

Figure 3. a) Hydrogen production from TxPP@TiO_2 hybrids loaded with 10 wt. % of polymer. b) Hydrogen evolution rate from TxPP@TiO_2 hybrids, analyzing the effect of polymer loading. Results from TiO_2 under the same conditions are included for comparative purposes. The estimated measurement error is 5 %.

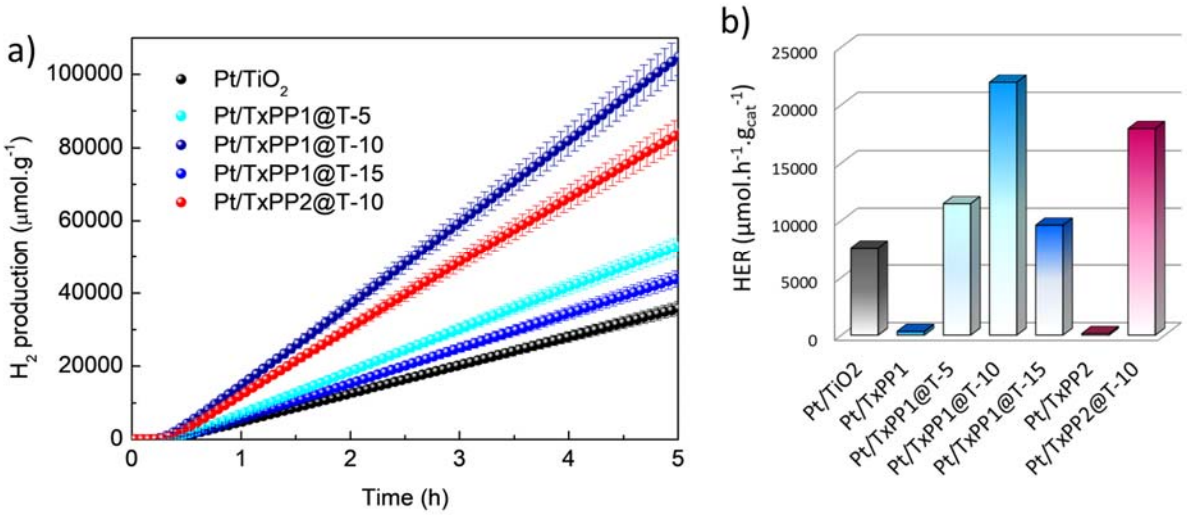

Figure 4. a) Hydrogen production and b) comparative of HER of Pt/TxPP1@TiO_2 at different polymer loading (blue points of different intensities) and Pt/TxPP2@T-10 (red point). Results from Pt/TiO_2 and Pt/TxPPX are included for comparative purposes. The estimated measurement error is 5%.

Noteworthy, these hybrid materials also show high photostability. The most active hybrid Pt/TxPP1@T-10 was continually irradiated during 21 hours showing a slightly loss of activity under 15 hours of irradiation (Figure S6) and intermittently during three on-off cycles of 4 hours each without loss of hydrogen production (Figure S7).

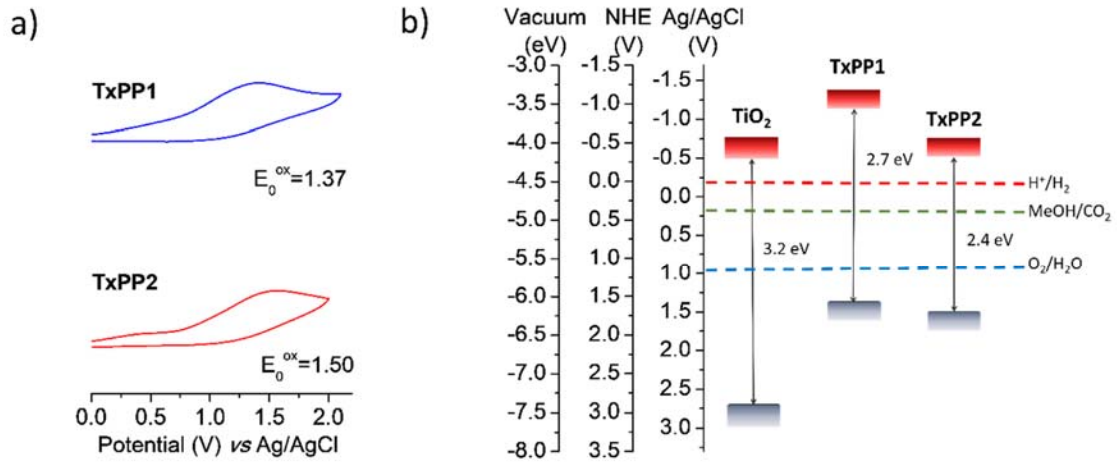

Figure 5. a) Cyclic voltammetry of TxPPs deposited on platinum, measured in acetonitrile containing 0.1M $TBAPF_6$ as supporting electrolyte. A platinum electrode acts as working electrode and the scan rate was 50 mVs^{-1}. b) VB/CV energy levels of TxPPs and TiO_2. Potential required for water splitting reaction and oxidation of methanol are included.

In order to clarify the differences in the photo-reactivity of both hybrid materials, understanding the electron charge mechanism operating, will be of fundamental importance. With this in mind, the relationship between the molecular and electronic structure of both truxene-polymers has been investigated. The band energy edges of TxPPs were determined by optical and electrochemical methods. Band gap energies were attained from the tauc plot as direct transition obtained by means of diffuse reflectance measurements (Figure S8 and Figure S9), the tauc plot as indirect transitions have also been calculated. Meanwhile, the conduction band (CB) was determined by cyclic

voltammetry (Figure 5a). Attending to these data, both conduction and valence band energy levels of CPPs based on truxene with respect to the valence and conduction band of TiO_2[42] have been located (Figure 5b). With these energy levels two kind of charge transfer mechanism could be possible (Figure 6). The first one corresponds to a type II heterojunction mechanism, where both polymer and TiO_2 absorb light and the polymer injects electrons from its CB level to the TiO_2 CB, being the TiO_2 the responsible of the reduction pathway (Figure 6a).[12] The second one is referred to a Z-scheme mechanism where, once a pair of excitons is generated in both materials, the electrons of TiO_2 CB are transferred to the polymer VB, being the polymer responsible of the reduction pathway (Figure 6b). In principle, a Z-Scheme charge transfer mechanism offers higher overall H_2 production than Type II heterojunction mechanism as it provides a higher energy gap between the reduction and oxidation pathway. Note that both mechanisms are valid for H_2 production and for the photoreduction of platinum. Platinum (0) nanoparticles will be deposited either over TiO_2 (Type II) or over the polymer surface (Z-Scheme) depending of the mechanism and it is over the Pt NPs where the reduction reaction takes place.

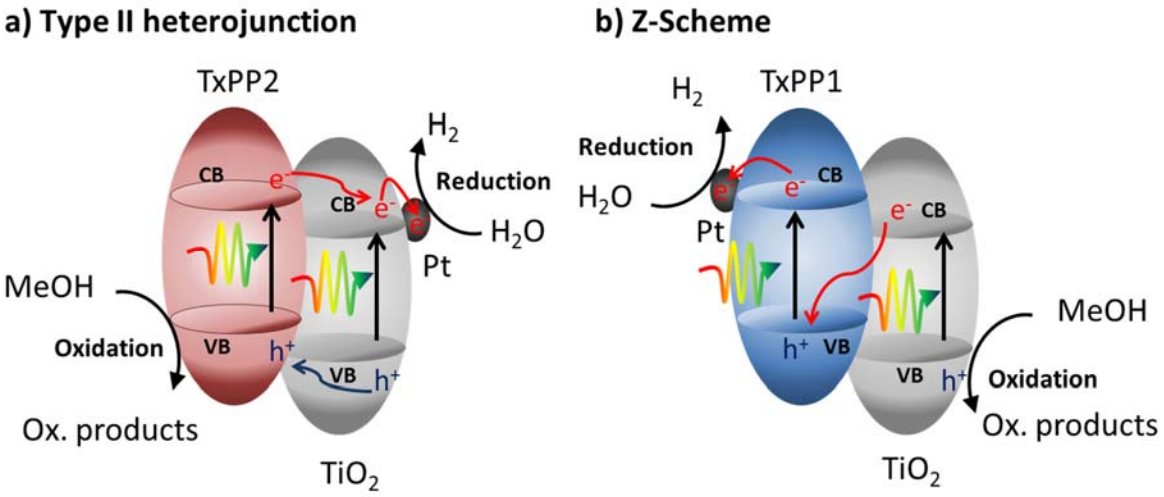

Figure 6. Plausible electron transfer mechanisms: a) type II heterojunction; b) Z-Scheme.

In order to gain insight in the electron transfer mechanism, photoluminescence and transient absorption experiments have been carried out. TiO_2 and TxPP1 show fluorescence emission properties in the solid state (Figure 7). When TxPP1@T-10 is analyzed under steady state conditions, the fluorescence emission of the TiO_2 is quenched (Figure 7a), whereas the fluorescence attributed to the polymer is enhanced. In order to discard a filter effect, due to absorption by the polymer fluorescence, we have performed time resolved fluorescence experiments. The quenching of the fluorescence emission of the TiO_2 is confirmed by a decrease in the TiO_2 average lifetime when it is forming part of the hybrid material (Figure 7b), while the TxPP1 fluorescence lifetime does not change (Figure 7c). This observation suggests that (in a Z-scheme electron transfer mechanism): the electron's population in the TiO_2 valence band decreases while conduction band's population of TxPP1 increases. However, the same experiment with TxPP2@T-10 show no change in the lifetime of TiO_2, (Figure 8) leading to conclude that in this case a type II charge transfer mechanism should be the responsible of the synergy between both materials. Note that in this case TxPP2 does not show fluorescence.

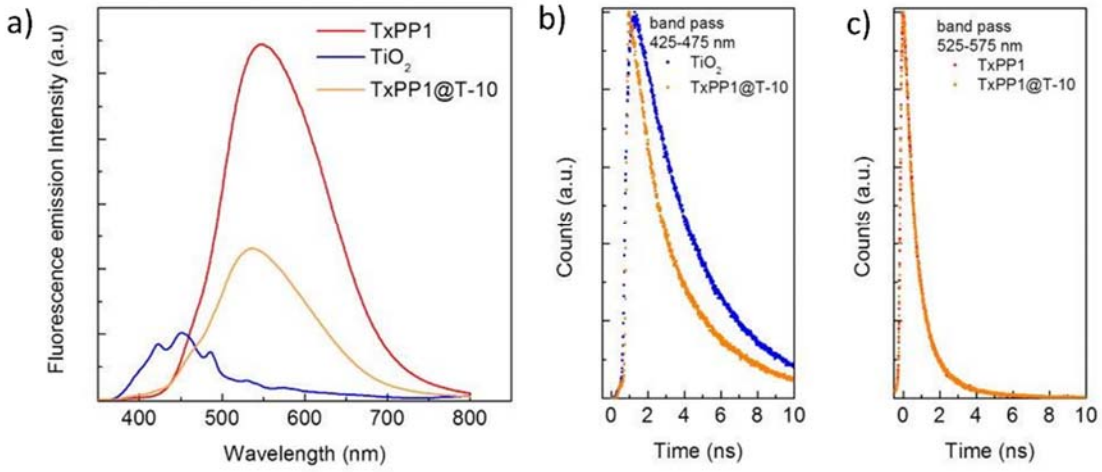

Figure 7. a) Steady state fluorescence emission of TiO_2 (blue line), TxPP1 (red line) and TxPP1@T-10 (orange line) in the same measurement conditions (solid state, λ_{exc}=300 nm, with a

cut off filter at 390 nm). b) Fluorescence lifetime of TiO_2 (blue) and TxPP1@T-10 (orange) exciting at λ_{exc}= 372 nm, 67 ps of laser pulse with a 425-475 nm band pass filter. c) Fluorescence lifetime of TxPP1 (red) and TxPP1@T-10 (orange) exciting at λ_{exc}=372 nm, 67ps of laser pulse with a 525-575 nm band pass filter.

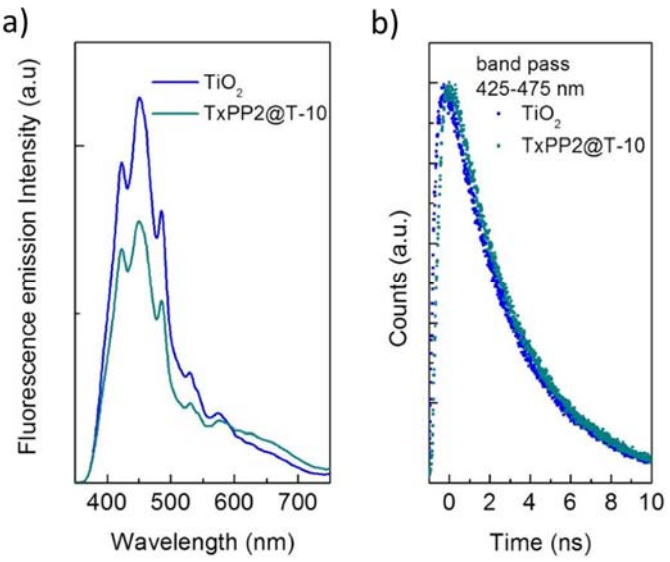

Figure 8. a) Steady state fluorescence emission of TiO_2 (blue line) and TxPP2@T-10 (dark cyan) in the same measurement conditions (solid state, λ_{exc}= 300 nm, with a cut off filter at 390 nm). Note that TxPP2 does not show fluorescence emission; B) Fluorescence lifetime of TiO_2 (blue) TxPP2@T-10 (dark cyan) exciting at λ_{exc}= 372 nm, 67ps of laser pulse with a 425-475 nm band pass filter.

A complementary approach to investigate and confirm the photophysical behavior of TxPP-TiO_2 hybrids was based on laser flash photolysis (LFP) experiments. Transient absorption experiments (TAS) are effective spectroscopy methods to detect the transients species generated by photon absorption.[37,38.] As a control, the decay trace for TiO_2 alone was measured, showing after excitation with a laser source on 355 nm, two major populations with a first shortest lifetime (τ = 47.50 ns) in the nanosecond scale and a second longer lifetime in the microsecond scale (τ = >1 μs) (Figure 9, black traces). On other hand, when TxPP2 or TxPP1 were submitted to LFP, no significant

signal was observed (Figure S10 Supporting Information); however, noticeable differences were detected for the TiO_2 signals in the presence both polymers (10%) depending on whether a polymer or other was monitored.

Interestingly, although both polymers show different behavior, in both cases a remarkable lifetime enhancement is observed when compared to TiO_2 alone. Thus, for TxPP2@T-10 polymer, an increase in the transient absorption was detected during the first nanoseconds after the laser pulse (Figure 9a, right side), accompanied with a small but significant delay in the lifetime profile. In addition, an enhancement in the shortest lifetime (τ = 56.35 ns, major population) is also observed, followed by an electron-hole recombination in the same time scale than that obtained for TiO_2. This result suggests that an electron transfer from the polymer to TiO_2 excited state is occurring (Figure 9c, red traces).

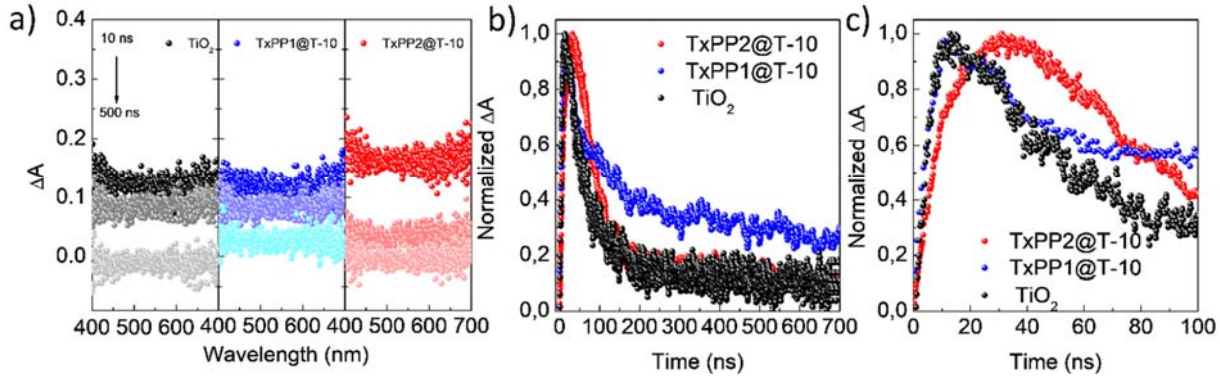

Figure 9. a) Transient absorption spectra obtained at different delay times after the laser pulse for TiO_2 (black), TxPP1@T-10 (blue) and TxPP2@T-10 (red) in aqueous suspension solutions under inert atmosphere. b) Decay traces at 460 nm (λ_{exc} = 355 nm) monitored at long time scale *ca.* 700 ns and c) monitored at short time scale *ca.* 100 ns.

On the other hand, TxPP1@T-10 shows no change in the shortest lifetime of the excited state's absorption (τ = 46.80 ns) and a longer lifetime in the microsecond scale up to 6 μs (Figure 9b, blue

traces and Figure S11 Supporting Information) when compared to bare TiO_2 or TxPP2@T-10. This outcome means that the photogenerated charge can migrate further before it decays back to the ground state leading to a more efficient electron–hole separation. This result is in accordance with data reported in literature, where for other semiconductors the presence of an electron acceptor (TxPP1 in our case), increases its TAS signal in the microsecond scale.[45] In summary, TAS studies combined with fluorescence results (Figures 7 and Figure 8), confirm a heterojunction type Z-scheme for TxPP1@T-10, and a heterojunction type II for TxPP2@T-10 and explain the higher photocatalytic activity of TxPP1@T-10 (Figure 3b). Both charge transfer mechanism can be understood considering the differences in the molecular structure of the constituent monomeric units in the polymers. Stacking interaction between neighboring units are expected to be more favorable in TxPP1 (with truxenes functionalized with less bulky methyl substituents), than in TxPP2 (with truxenes functionalized with sterically demanding benzyl groups), providing a more efficient pathway for charge migration.[24] This effect could lead to a better charge separation and more efficient interface with the TiO_2.

As we explained above, if the charge transfer mechanism runs by a Z-Scheme, the reduction pathway is located in the polymer surface while the oxidation pathway occurs in the titania surface. To confirm this point, a transmission electron microscopy (TEM) image of the hybrid TxPP1@T-10 loaded with Pt has been recorded (Figure 10a). As the platinum nanoparticles are deposited by photoreduction of a platinum precursor in a Z-Scheme mechanism, they should be deposited in the polymer surface. Figures 10b shows the same image field but recorded by scanning transmission electron microscopy (STEM) in high-angle annular dark field (HAADF) mode where the brilliant points presumably correspond to the platinum nanoparticles. Meanwhile, Figures 10d-10g depict a mapping analysis for Ti, O, C and Pt elements by means of energy-dispersive X-ray (EDX)

analysis, which confirms the presence of platinum nanoparticles mostly in the polymer surface. However, TEM image of Pt/TxPP2@T-10 shows the absence of platinum in the polymer surface, corroborating the charge transfer mechanism type II (Figure S12b at supporting information).

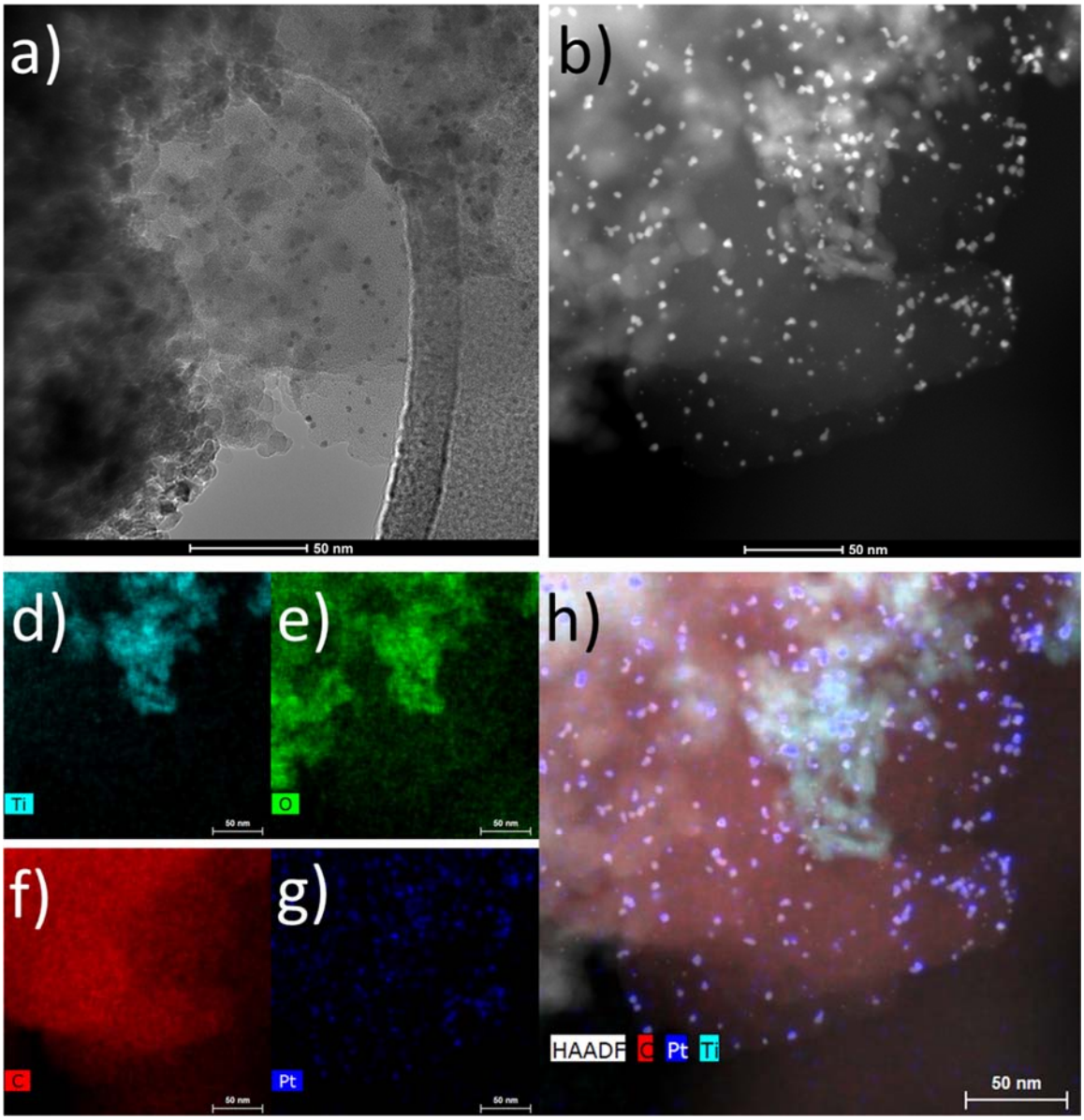

Figure 10. a) TEM image; b) High-angle annular dark field (HAADF) image by STEM; d)-g) element mapping by EDX of Ti, O, C and Pt, respectively; h) Overlapping of HAADF Image and EDX images. All of them regarding to Pt/TxPP1@T-10 (loading Pt by photoreduction) sample.

CONCLUSIONS

This work shows the ability of porous organic polymers based on truxene moieties (TxPP1 and TxPP2) and their corresponding TxPP@TiO_2 hybrids to photocatalytically produce hydrogen from water under UV-Vis irradiation using methanol as sacrificial agent. A clear synergic effect between the polymers and titania is observed in the hydrogen production, which is enhanced when Pt nanoparticles are used as co-catalyst. Differences in the truxene scaffold lead to different charge transfer mechanism (between polymer and TiO_2), that was elucidated by photoluminescence and transient absorption experiments, being Z-scheme for the most active composite (TxPP1@T-10) and type II heterojunction for the less active (TxPP2@T-10). In particular, Pt/TxPP1@T-10 showed the highest *HER* (21000 $\mu mol.g^{-1}.h^{-1}$) reported so far for hybrid materials based on porous polymers and TiO_2.

In conclusion, in this manuscript we have established useful structure-activity relationships of great interest in the development of new hybrid materials with highly efficient photocatalytic properties with the aim of optimizing the hydrogen production from water, one of the most currently needed challenge to stop relying on fossil fuels.

EXPERIMENTAL

Synthesis of Truxene-based porous organic polymers.

In a typical reaction, under inert atmosphere, substituted truxene (0.5 mmol) was dissolved in 15 mL anhydrous dichloromethane, then, 1 g of anhydrous aluminum chloride was added under N_2 atmosphere with stirring and heated at 40 ºC for 24-48 h. The resulting black solid was filtered and thoroughly washed with CH_2Cl_2, HCl (2 mL HCl/ 50 mL H_2O), THF and refluxing methanol, to obtain the corresponding yellow-orange solid (>90 % yield).

Preparation of hybrids polymer@TiO_2.

TiO_2 was previously calcined in air at 400 °C for 4 hours in order to remove all the possible organic impurities. Both TiO_2 and truxene-polymer (1, 5, 10 or 15 wt. %) were dispersed in a

mixture of water/acetonitrile (1:1 v/v) and sonicated for 15 min; afterward, the solvents were removed using a rotary evaporator at 50 ºC and the mixture was crushed in a mortar. Catalysts are labelled as polymer@T-x, where x refers to the polymer loading (1, 5, 10 or 15 wt. %).

Photocatalytic activity test.

Photocatalytic hydrogen production experiments were carried out in semi-batch mode in a tightly closed Pyrex glass reactor containing 1 L of a 10 vol. % methanol aqueous solution and 100 mg of catalyst. The reactor was irradiated with a medium-pressure Hg immersion lamp kept at 20 °C by means of a water circulation chiller (Huber Minichiller NR). Ar was bubbled through the solution at a flowrate of 60 sccm in order to remove air and carry the product gases for analysis in a dual-channel Agilent micro-GC 450 equipped with MS5A PLOT and PoraPLOT U columns and TCD detectors.

The platinum nanoparticles where deposited by photoreduction of H_2PtCl_6 precursor. Thus, 100 mg of polymer@T-x hybrid was dispersed on 1 L of a mixture water: MeOH 9:1 v/v (same configuration vide infra). The dispersion was deaerated under an Argon current of 60 mL cm^{-3} and finally, 236 µL of a 4.25 gL^{-1} solution of H_2PtCl_6 were added and then UV irradiated. Note, that this experiment is used directly to measure the hydrogen production.

Characterization techniques

Ultraviolet–visible diffuse reflectance spectra (UV– Vis DRS). Ultraviolet–visible diffuse reflectance spectra (UV– Vis DRS) of the solid powdered samples were obtained by a Perkin Elmer Lambda 1050 UV/Vis/NIR spectrometer and the reflectance spectra were plotted as the Kubelka Munk function (Equation 1):

$$F(R) = \frac{(1-R)^2}{2R} \quad \text{.....Equation 1}$$

To measure the optical band gap tauc plot as direct $(F(R)*h\nu)^2$ vs. hν) and indirect $(F(R)*h\nu)^{1/2}$ vs. hν) transition have been depicted.

Fluorescence emission spectra. Experiments for solid powdered samples were carried out with a Fluorescence Spectrometer Perkin Elmer LS 55, with an excitation wavelength of 300 nm and using a cut-off filter at 390 nm in front-face mode. Lifetime measurements were carried out by Time Correlated Single Photon Counting (TCSPC) with a Mini-τ equipment from Edinburgh Instruments. A excitation source we used a laser diode (model EPL375) at 372 nm, with a pulse width of 61.2 ps at a repetition rate of 1 MHz in the presence of two kind of band pass filter 425-475 nm and 525-575 nm, respectively.

Laser Flash Photolysis (LFP). Experiments for aqueous samples were performed with a LP980 from Edinburgh Co (LP980-K) instrument. The system includes as a pump source an optical parametric oscillator (OPO) pumped by the third harmonic of a Nd: YAG laser from EKSPLA. The measurements were monitored at 355 nm as excitation wavelength with single low energy pulses of 1 mJ/pulse of ca. 5 ns duration and 10 Hz as repetition rate. The white probe light is provided by a pulsed xenon flash lamp (150 W) with a duration of the probe of 250 us. This probe light goes through the sample and then a monochromator (TMS302-A, grating 150 lines/mm) that disperses the probe light before to reach a PMT detector (Hamamatsu Photonics) to obtain the transient picture. Before the acquisitions, the samples were diluted in aqueous solutions and sonicated to disperse the polymers. The samples were bubbled with N_2 for 15 minutes and measured with an absorbance of ~0.3 at λ_{exc} = 355 nm. All transient spectra and decay traces were recorded at room temperature using 10 x 10 mm^2 quartz cells.

Cyclic voltamperometry and photovoltage measurements. A three-electrode cell configuration was used. Current and voltage signals were measured through an Autolab PGSTAT204

potentiostat/galvanostat station. A paste was prepared mixing 5 mg of each Truxene-CPPs with 45µL of Nafion perflorinated resin solution (5% wt. in mixture of lower aliphatic alcohols and water, 45%) and 450 µL of isopropanol. After that, this paste was deposited and dried on the platinum working electrode. A platinum wire was used as the counter electrode and an Ag wire electrode as the pseudo-reference (calibrated with ferrocene). 0.1 M $TBAPF_6$ in acetonitrile was utilized as electrolyte.

Scanning Electron Microscopy (SEM). The images were taken with a TM-1000 tabletop microscope (HITACHI). The samples were sprinkle on a carbon double-sided tape without further metalation.

Transmission electron microscopy (TEM). Experiment for the TxPP1@TiO_2 10% loaded with 1wt% Pt were carried out with a FEG S/TEM (Talos F200X, FEI) equipment provided with a chemical analysis system via energy-dispersive X-ray spectroscopy (EDS), a digital CMOS camera able to acquire images with a maximum resolution of 4×4 k. The equipment offers a TEM point resolution ≤ 0.25 nm at 200 kV, information threshold ≤ 0.12 nm at 200 kV, and a STEM-HAADF at 200 kV ≤ 0.16 nm. On the other hand, the image for TxPP2@TiO2 10% loaded with 1wt. % Pt was carried out with a JEOL JEM 2100 equipment with chemical analysis system via energy-dispersive X-ray spectroscopy (EDS), a camera CCD ORIUS SC1000 (Model 832) with a TEM point resolution ≤ 0.25 nm.

ASSOCIATED CONTENT

Supporting Information

Experimental procedures, analytical data and spectroscopical characterizations.

AUTHOR INFORMATION

Corresponding author

e-mail for M.L.: marta.liras@imdea.org

e-mail for BGL: bgl@icmm.csic.es
e-mail for M.I.: marta.iglesias@icmm.csic.es

ORCID

Marta Iglesias: 0000-0001-7373-4927
Berta Gómez-Lor: 0000-0002-2995-9624
Marta Liras: 0000-0002-1724-1586
Víctor A. de la Peña O´Shea: 0000-0001-5762-4787
Mariam Barawi: 0000-0001-5719-9872
Antonio Valverde-González: 0000-0002-2982-6389
Carmen G. López Calixto: 0000-0002-2771-9563

Notes

The authors declare no competing financial interest

Author Contributions

The manuscript was written through contributions of all authors. All authors have given approval to the final version of the manuscript.

ACKNOWLEDGMENT

Authors acknowledge to MINECO/AEI/FEDER, UE of Spain (Projects MAT2017-82288-C2-2-P, CTQ2016-78557-R and ENE2016-79608-C2-1-R) and regional government of "Comunidad de Madrid" and European Structural Funds for their financial support to FotoArt-CM project (S2018/NMT-4367). AVG thanks Ministerio de Educación y Formación Profesional for FPU17/03463, M. L and M. B thank to MINECO and European Social Fund for a Ramón y Cajal grant (RyC-2015-18677) and Juan de la Cierva Formación grant (FJCI-2016-30567) respectively.

References

(1) Takata, T.; Domen, K. Particulate Photocatalysts for Water Splitting: Recent Advances and Future Prospects. *ACS Energy Lett.* **2019**, *4* (2), 542–549.

(2) Wang, H.; Zhang, L.; Chen, Z.; Hu, J.; Li, S.; Wang, Z.; Liu, J.; Wang, X. Semiconductor Heterojunction Photocatalysts: Design, Construction, and Photocatalytic Performances. *Chem. Soc. Rev.* **2014**, *43* (15), 5234–5244.

(3) Cao, S.; Yu, J. g-C_3N_4-Based Photocatalysts for Hydrogen Generation. *J. Phys. Chem. Lett.* **2014**, *5* (12), 2101–2107.

(4) Schneider, J.; Matsuoka, M.; Takeuchi, M.; Zhang, J.; Horiuchi, Y.; Anpo, M.; Bahnemann, D. W. Understanding TiO_2 Photocatalysis: Mechanisms and Materials. *Chem. Rev.* **2014**, *114*, 9919–9986.

(5) Park, H.; Park, Y.; Kim, W.; Choi, W. Surface Modification of TiO_2 Photocatalyst for Environmental Applications. *J. Photochem. Photobiol. C Photochem. Rev.* **2013**, *15* (1), 1–20.

(6) Serpone, N.; Emeline, A. V.; Ryabchuk, V. K.; Kuznetsov, V. N.; Artem'Ev, Y. M.; Horikoshi, S. Why Do Hydrogen and Oxygen Yields from Semiconductor-Based Photocatalyzed Water Splitting Remain Disappointingly Low? Intrinsic and Extrinsic Factors Impacting Surface Redox Reactions. *ACS Energy Lett.* **2016**, *1* (5), 931–948.

(7) Wang, X.; Maeda, K.; Thomas, A.; Takanabe, K.; Xin, G.; Carlsson, J. M.; Domen, K.; Antonietti, M. A Metal-Free Polymeric Photocatalyst for Hydrogen Production from Water under Visible Light. *Nat. Mater.* **2008**, *8* (1), 76–80.

(8) Shi, J. On the Synergetic Catalytic Effect in Heterogeneous Nanocomposite Catalysts. *Chem. Rev.* **2013**, *113* (3), 2139–2181.

(9) Chen, C.; Ma, W.; Zhao, J. Semiconductor-Mediated Photodegradation of Pollutants under

Visible-Light Irradiation. *Chem. Soc. Rev.* **2010**, *39* (11), 4206–4219.

(10) Wang, L.; Zhang, Y.; Chen, L.; Xu, H.; Xiong, Y. 2D Polymers as Emerging Materials for Photocatalytic Overall Water Splitting. *Adv. Mater.* **2018**, *30* (48), 1–12.

(11) Sachs, M.; Sprick, R. S.; Pearce, D.; Hillman, S. J.; Monti, A.; Guilbert, A. A. Y.; Brownbill, N. J.; Dimitrov, S.; Blanc, F.; Zwijnenburg, M. A.; Nelson, J; Durrant, J. R.; Cooper, A. I. Understanding Structure-Activity Relationships in Linear Polymer Photocatalysts for Hydrogen Evolution. *Nat. Commun.* **2018**, 1–11.

(12) Liras, M.; de la Peña O'Shea, V. A.; Liras, M. Hybrid Materials Based on Conjugated Polymers and Inorganic Semiconductors as Photocatalysts: From Environmental to Energy Applications. *Chem. Soc. Rev.* **2019**, *48* (5454–5487).

(13) Mothika, V. S.; Sutar, P.; Verma, P.; Das, S.; Pati, S. K.; Maji, T. K. Regulating Charge-Transfer in Conjugated Microporous Polymer for Photocatalytic Hydrogen Evolution. *Chem. - A Eur. J.* **2019**, *25*, 3867–3874.

(14) Meier, C. B.; Clowes, R.; Berardo, E.; Jelfs, K. E.; Zwijnenburg, M. A.; Sprick, R. S.; Cooper, A. I. Structurally Diverse Covalent Triazine-Based Framework Materials for Photocatalytic Hydrogen Evolution from Water. *Chem. Mater.* **2019**, *31*, 8830–8838.

(15) Lan, Z.; Ren, W.; Chen, X.; Zhang, Y.; Wang, X. Conjugated Donor-Acceptor Polymer Photocatalysts with Electron-Output " Tentacles " for Efficient Hydrogen Evolution. *Appl. Catal. B Environ.* **2019**, *245* (December 2018), 596–603.

(16) Chen, J.; Tao, X.; Tao, L.; Li, H.; Li, C.; Wang, X.; Li, C.; Li, R.; Yang, Q. Novel Conjugated Organic Polymers as Candidates for Visible-Light-Driven Photocatalytic

Hydrogen Production. *Appl. Catal. B Environ.* **2019**, *241* (June 2018), 461–470.

(17) Liras, M.; Iglesias, M.; Sánchez, F. Conjugated Microporous Polymers Incorporating BODIPY Moieties as Light-Emitting Materials and Recyclable Visible-Light Photocatalysts. *Macromolecules* **2016**, *49*, 1666–1673.

(18) Liras, M.; Pintado-Sierra, M.; Iglesias, M.; Sánchez, F. Deprotection Strategy of a BODIPY Conjugated Porous Polymer to Obtain Heterogeneous (Dipyrrin)(Bipyridine)Ruthenium(II) Visible Light Photocatalyst. *J . Mater. Chem. A* **2016**, *4*, 17274–17278.

(19) López-Calixto, C. G.; Cabrera, S.; Pérez-Ruiz, R.; Barawi, M.; Alemán, J.; de la Peña O'Shea, V. A.; Liras, M. Conjugated Porous Polymer Based on BOPHY Dyes as Photocatalyst under Visible Light. *Appl. Catal. B Environ.* **2019**, 117933.

(20) Goubard, F.; Dumur, F. Truxene: A Promising Scaffold for Future Materials. *RSC Adv.* **2015**, *5* (5), 3521–3551.

(21) Guadalupe, J.; Ray, A. M.; Maya, E. M.; Gómez-Lor, B.; Iglesias, M. Truxene-Based Porous Polymers: From Synthesis to Catalytic Activity. *Polym. Chem.* **2018**, *9* (36), 4585–4595.

(22) Battula, V. R.; Singh, H.; Kumar, S.; Bala, I.; Pal, S. K.; Kailasam, K. Natural Sunlight Driven Oxidative Homocoupling of Amines by a Truxene-Based Conjugated Microporous Polymer. *ACS Catal.* **2018**, *8* (8), 6751–6759.

(23) de Frutos, O.; Granier, T.; Gómez-Lor, B.; Jiménez-Barbero, J.; Monge, A.; Gutie, E.; Echavarren, A. M. Synthesis and Self-Association of Syn-5,10,15-Trialkylated Truxenes. *Chem. Eur. J.* **2002**, *8*, 2879–2890.

(24) De Frutos, Ó.; Gómez-Lor, B.; Granier, T.; Monge, M. Á.; Gutiérrez-Puebla, E.; Echavarren, A. M. Syn-Trialkylated Truxenes: Building Blocks that Self-Associate by Arene Stacking. *Angew. Chemie - Int. Ed.* **1999**, *38* (1–2), 204–207.

(25) Guiglion, P.; Butchosa, C.; Zwijnenburg, M. A. Polymer Photocatalysts for Water Splitting: Insights from Computational Modeling. *Macromol. Chem. Phys.* **2016**, *217* (3), 344–353.

(26) Bildirir, H.; Paraknowitsch, J. P.; Thomas, A. A Tetrathiafulvalene (TTF)-Conjugated Microporous Polymer Network. *Chem. - A Eur. J.* **2014**, *20* (31), 9543–9548.

(27) Jiang, J.-X.; Su, F.; Trewin, A.; Wood, C. D.; Campbell, N. L.; Niu, H.; Dickinson, C.; Ganin, A. Y.; Rosseinsky, M. J.; Khimyak, Y. Z.; Cooper, A. I. Conjugated Microporous Poly(Aryleneethynylene) Networks. *Angew. Chemie Int. Ed.* **2007**, *46* (45), 8574–8578.

(28) Ran, J.; Jaroniec, M.; Qiao, S. Z. Cocatalysts in Semiconductor-Based Photocatalytic CO_2 Reduction: Achievements, Challenges, and Opportunities. *Adv. Mater.* **2018**, *30* (7), 1–31.

(29) Collado, L.; Reynal, A.; Fresno, F.; Barawi, M.; Escudero, C.; Perez-Dieste, V.; Coronado, J. M.; Serrano, D. P.; Durrant, J. R.; de la Peña O'Shea, V. A. Unravelling the Effect of Charge Dynamics at the Plasmonic Metal/Semiconductor Interface for CO_2 Photoreduction. *Nat. Commun.* **2018**, *9* (1), 4986.

(30) Tasbihi, M.; Fresno, F.; Simon, U.; Villar-García, I. J.; Pérez-Dieste, V.; Escudero, C.; de la Peña O'Shea, V. A. On the Selectivity of CO_2 Photoreduction towards CH_4 Using Pt/TiO_2 Catalysts Supported on Mesoporous Silica. *Appl. Catal. B Environ.* **2018**, *239* (July), 68–76.

(31) Lan, Z. A.; Ren, W.; Chen, X.; Zhang, Y.; Wang, X. Conjugated Donor-Acceptor Polymer

Photocatalysts with Electron-Output “Tentacles” for Efficient Hydrogen Evolution. *Appl. Catal. B Environ.* **2019**, *245* (January), 596–603.

(32) Xu, Y.; Mao, N.; Zhang, C.; Wang, X.; Zeng, J.; Chen, Y.; Wang, F.; Jiang, J. X. Rational Design of Donor-π-Acceptor Conjugated Microporous Polymers for Photocatalytic Hydrogen Production. *Appl. Catal. B Environ.* **2018**, *228* (January), 1–9.

(33) Sprick, R. S.; Bai, Y.; Guilbert, A. A. Y.; Zbiri, M.; Aitchison, C. M.; Wilbraham, L.; Yan, Y.; Woods, D. J.; Zwijnenburg, M. A.; Cooper, A. I. Photocatalytic Hydrogen Evolution from Water Using Fluorene and Dibenzothiophene Sulfone-Conjugated Microporous and Linear Polymers. *Chem. Mater.* **2019**, *31* (2), 305–313.

(34) Schwarz, D.; Acharja, A.; Ichangi, A.; Lyu, P.; Opanasenko, M. V.; Goßler, F. R.; König, T. A. F.; Čejka, J.; Nachtigall, P.; Thomas, A.; Bojdys, M. J. Fluorescent Sulphur- and Nitrogen-Containing Porous Polymers with Tuneable Donor–Acceptor Domains for Light-Driven Hydrogen Evolution. *Chem. - A Eur. J.* **2018**, *24* (46), 11916–11921.

(35) Hou, H. J.; Zhang, X. H.; Huang, D. K.; Ding, X.; Wang, S. Y.; Yang, X. L.; Li, S. Q.; Xiang, Y. G.; Chen, H. Conjugated Microporous Poly(Benzothiadiazole)/TiO_2 Heterojunction for Visible-Light-Driven H_2 Production and Pollutant Removal. *Appl. Catal. B Environ.* **2017**, *203*, 513–517.

(36) Yang, Q.; Peng, P.; Xiang, Z. Covalent Organic Polymer Modified TiO_2 Nanosheets as Highly Efficient Photocatalysts for Hydrogen Generation. *Chem. Eng. Sci.* **2017**, *162*, 33–40.

(37) Han, C.; Wang, Y.; Lei, Y.; Wang, B.; Wu, N.; Shi, Q.; Li, Q. In Situ Synthesis of Graphitic-

C_3N_4 Nanosheet Hybridized N-Doped TiO_2 Nanofibers for Efficient Photocatalytic H_2 Production and Degradation. *Nano Res.* **2015**, *8* (4), 1199–1209.

(38) Karthik, P.; Vinoth, R.; Selvam, P.; Balaraman, E.; Navaneethan, M.; Hayakawa, Y.; Neppolian, B. A Visible-Light Active Catechol–Metal Oxide Carbonaceous Polymeric Material for Enhanced Photocatalytic Activity. *J. Mater. Chem. A* **2017**, *5* (1), 384–396.

(39) Xiang, Y.; Wang, X.; Zhang, X.; Hou, H.; Dai, K.; Huang, Q.; Chen, H. Enhanced Visible Light Photocatalytic Activity of TiO_2 Assisted by Organic Semiconductors: A Structure Optimization Strategy of Conjugated Polymers. *J Mater Chem A* **2018**, *6*, 153–159.

(40) Xiao, J.; Luo, Y.; Yang, Z.; Xiang, Y.; Zhang, X.; Chen, H. Synergistic Design for Enhancing Solar-to-Hydrogen Conversion over a TiO_2 -Based Ternary Hybrid. *Catal. Sci. Technol.* **2018**, *8* (9), 2477–2487.

(41) Chen, B.; Wang, X.; Dong, W.; Zhang, X.; Rao, L.; Chen, H.; Huang, D.; Xiang, Y. Enhanced Light-Driven Hydrogen-Production Activity Induced by Accelerated Interfacial Charge Transfer in Donor–Acceptor Conjugated Polymers/TiO_2 Hybrid. *Chem. - A Eur. J.* **2019**, *25* (13), 3362–3368.

(42) Kapilashrami, M.; Zhang, Y.; Liu, Y.-S.; Hagfeldt, A.; Guo, J. Probing the Optical Property and Electronic Structure of TiO2 Nanomaterials for Renewable Energy Applications. *Chem. Rev.* **2014**, *114* (19), 9662–9707.

(43) Baldoví, H. G.; Ferrer, B.; Álvaro, M.; García, H. Microsecond Transient Absorption Spectra of Suspended Semiconducting Metal Oxide Nanoparticles. *J. Phys. Chem. C* **2014**, *118* (17), 9275–9282.

(44) Tang, J.; Durrant, J. R.; Klug, D. R. Mechanism of Photocatalytic Water Splitting in TiO_2. Reaction of Water with Photoholes, Importance of Charge Carrier Dynamics, and Evidence for Four-Hole Chemistry. *J. Am. Chem. Soc.* **2008**, *130* (42), 13885–13891.

(45) Aiga, N.; Jia, Q.; Watanabe, K.; Kudo, A.; Sugimoto, T.; Matsumoto, Y. Electron-Phonon Coupling Dynamics at Oxygen Evolution Sites of Visible-Light-Driven Photocatalyst: Bismuth Vanadate. *J. Phys. Chem. C* **2013**, *117* (19), 9881–9886.

Table of Contents Graphic